is given by,

$$\Upsilon(t) = \int_{-\infty}^{+\infty} \Omega(\lambda)\Omega(\lambda+t)\,d\lambda$$
$$= E_\circ^2 \Delta T \sum_{k=0}^{2} I_k \exp\{-a_k[(t-t_\circ)/\Delta T]^2\}, \quad (2)$$

where

$$I_0 = \frac{1}{\sqrt{2}(1-\alpha)^2}, \qquad a_0 = \frac{\pi}{2}, \quad (3)$$

$$I_1 = \frac{\alpha}{\sqrt{2}(1-\alpha)^2}, \qquad a_1 = \frac{\pi\alpha^2}{2}, \quad (4)$$

$$I_2 = \frac{-2\alpha}{(1-\alpha)^2(1+\alpha^2)^{1/2}}, \qquad a_2 = \frac{\pi\alpha^2}{(1+\alpha^2)}. \quad (5)$$

The Fourier transform of the GG pulse is

$$\Lambda(f) = \int_{-\infty}^{+\infty} \Omega(t)\exp\{-j2\pi ft\}\,dt$$
$$= \frac{E_\circ \exp\{-j2\pi t_\circ(f/\Delta f)\}}{\Delta f(1-\alpha)}\left[\exp\{-\pi(f/\Delta f)^2\}\right.$$
$$- \left.\exp\{-(\pi/\alpha^2)(f/\Delta f)^2\}\right], \quad (6)$$

where $\Delta f = 1/\Delta T$ is the effective frequency bandwidth of the GG pulse. The time variation of the normalized GG pulse $\Omega(t)/E_\circ$, the normalized autocorrelation function $\Upsilon(t)/\Upsilon(0)$, and the energy density spectrum $\Psi(f) = |\Lambda(f)|^2$ are shown in Fig. 1 for the values of the scaling factor $\alpha = 0$ (dotted line), $\alpha = 0.3$ (dashed line), $\alpha = 0.6$ (dashed-dotted line), and $\alpha = 1.2$ (solid line). For $\alpha = 0$, $\Omega(t)$ is an ideal Gaussian pulse and its energy density spectrum in Fig. 1c (dotted line) includes a dc component at the normalized frequency $f/\Delta f = 0$. The GG pulse is a convenient signal model for developing the theory and analysis of impulse radar and communications.

Impulse-Array Beamforming

An active array beamforming system for UWB impulse radar is shown in Fig. 2. The $2m+1$ equally spaced array elements have dual role as radiators and as sensors for emitting and receiving electromagnetic impulses. The transmitter module includes pulse generators and driving circuits (PG-DC$_i$), $i = 0, \pm1, \pm2, \ldots, \pm m$, for switching and delivering high peak-power transient currents to the array elements. Each array element is also connected to the receiver module via a duplexer, which isolates the receiver during the transmitting mode of the antenna array system. The receiver module is a beam forming network consisting of $2m+1$ sliding correlators (SC$_i$), Fourier transform processors (FTP$_i$), and a summer circuit (SUM). Proper shielding is necessary for all the equipment in the transmitter and the receiver modules for protection against mutual coupling.

Let the GG pulse $\Omega(t)$ given in (1) be radiated by the array elements in Fig. 2. A point scatterer in the far field at an angle ϕ with respect to the array axis reflects back to the antenna array a waveform having the time variation

$$\Omega_T(t,\phi) = \sum_{i=-m}^{+m} \Omega(t-\tau_i(\phi)), \quad (7)$$

where the normalized propagation delay

$$\tau_i(\phi)/\Delta T = (id/c\Delta T)\sin\phi$$
$$= (i/2m)\rho\sin\phi, \quad (8)$$

and

$$\rho = 2md/c\Delta T = L/c\Delta T = L\Delta f/c. \quad (9)$$

In (8) and (9), ρ is referred to as the *spatial frequency bandwidth*, d is the separation distance between adjacent array elements, and $L = 2md$ is the array length. For antenna array with a large number of elements, $m \gg 1$, the summation in (7) can be approximated by an integral with the help of the following substitutions: $\eta = i/2m, d\eta = d(i/2m)$, and for $i - \pm m \to -1/2 \le \eta \le +1/2$. The integral form of $\Omega_T(t,\phi)$ is expressed as follows,

$$\Omega_T(t,\phi) \approx 2m\int_{-1/2}^{+1/2} \Omega(t-\eta\rho\sin\phi)\,d\eta \quad (10)$$

With the help of (6), the Fourier transform of $\Omega_T(t,\phi)$ results in the amplitude-spectral-density function

$$\Lambda_T(f,\phi) = 2m\Lambda(f)\frac{\sin[\pi\rho(f/\Delta f)\sin\phi]}{\pi\rho(f/\Delta f)\sin\phi}$$
$$= 2m\Lambda(f)\mathrm{sinc}[\pi\rho(f/\Delta f)\sin\phi]. \quad (11)$$

During the receiving mode of the beamforming system in Fig. 2, the arriving wavefront is transduced by the array elements into voltage signals with the time variation $\Omega_T(t-\tau_i(\phi)), i = 0, \pm1, \pm2, \ldots, \pm m$. Each voltage signal is passed through the SC$_i$ to be correlated by a replica of the radiated GG pulse $\Omega(t)$. The correlation process yields maximum signal-to-noise ratio for the case of additive white Gaussian noise. The voltage signal from the SC$_i$ is then transformed into the frequency domain by the FTP$_i$ to result in the energy density spectrum of the received signal. This transformation is convenient for *space-frequency* analysis of impulse waveforms formulated at the output of the beamforming system.

In principle, each sliding correlator SC$_i$ in Fig. 2 can be regarded as a matched filter having a transfer function $\Lambda^*(f)$, where the asterisk denotes complex conjugate. In analogy to (7) and (11), the energy-spectral-density function at the output of SUM in Fig. 2 can be expressed as follows,

$$\Psi_T(f,\phi) = \Lambda(f)\Lambda^*(f)\{2m\mathrm{sinc}[\pi\rho(f/\Delta f)\sin\phi]\}^2$$
$$= \Psi(f)\left[H_A(f,\phi)\right]^2 \quad (12)$$

In (12), $\Psi(f) = |\Lambda(f)|^2 = \Lambda(f)\Lambda^*(f)$ is the energy density spectrum of the radiated GG pulse, and

$$H_A(f,\phi) = 2m\text{sinc}[\pi\rho(f/\Delta f)\sin\phi] \qquad (13)$$

is the transfer function of the array beamforming system in Fig. 2. In the case of a complex target that is composed of a finite number of scattering centers, and having a transfer function $H_T(f,\phi)$, the spectrum of the received signal at the output of SUM in the array system of Fig. 2 can be expressed as follows,

$$\widetilde{\Psi}_T(f,\phi) = \Psi(f)H_T(f,\phi)\left[H_A(f,\phi)\right]^2. \qquad (14)$$

The energy-spectral-density function $\Psi_T(f,\phi)$ given in (12) is plotted in Fig. 3 as a function of normalized frequency $f/\Delta f$, for the values of $\alpha = 0.5$, $\rho = 100$, and the angle of incidence (a) $\phi = 0°$, (b) $\phi = 2°$, (c) $\phi = 4°$, and (d) $\phi = 8°$. For on axis reception, $\phi = 0°$, the energy spectrum $\Psi_T(f,0) = \Psi(f)$. For off-axis reception, $\phi > 0°$, the energy spectrum $\Psi_T(f,\phi)$ at the output of SUM in Fig. 2 is a distorted (or modulated) version of the radiated energy spectrum $\Psi(f)$. The different modulation patterns, or directional distortions, shown in Fig. 3 can be regarded as useful information for direction finding and electronic beam steering. According to Fig. 3, the frequency of oscillation in the modulated spectrum $\Psi_T(f,\phi)$ is an increasing function of the angle ϕ. Hence, a measure of the frequency of oscillation results in an estimate, $\hat{\phi}$, of the angle of incidence ϕ. This estimate can then be used to calculate the required delay time for each array element so that a main beam can electronically be steered into the direction of the signal source, as in the case of *retro-directive array systems*.

The beamforming system in Fig. 2 can be advanced to operate as a retro-directive array system by employing a variable delay circuit (VDC_i) at each array element, and having them controlled by a delay adjustment computer (DAC). The output signal of SUM will be passed to the DAC to calculate the estimate $\hat{\phi}$ and adjust, accordingly, the delay of each VDC_i to achieve beam steering.

Directivity Energy Pattern

For impulse waveforms, the directivity energy pattern $W(\phi)$ of the beamforming system in Fig. 2 can be defined in terms of the ratio

$$W(\phi) = U(\phi)/U(0), \qquad (15)$$

where

$$U(\phi) = \int_0^\infty (|\Lambda(f)|\text{sinc}[\pi\rho(f/\Delta f)\sin\phi])^2\, df \qquad (16)$$

is the energy of the received signal at the output of SUM, and

$$U(0) = \int_0^\infty |\Lambda(f)|^2\, df, \qquad (17)$$

The energy pattern $W(\phi)$ is plotted in Fig. 4 for the values of $\alpha = 0.5$, and $\rho = 10$ (dotted line), $\rho = 20$ (dashed line), $\rho = 30$ (dashed-dotted line), and $\rho = 40$ (solid line). The half-energy-point beamwidth of $W(\phi)$, which defines the resolution angle, is narrower for the larger values of the spatial frequency bandwidth ρ. Hence, the resolution angle, ε, for the energy pattern $W(\phi)$ is inversely proportional to ρ, and can be expressed as follows,

$$\varepsilon = K/\rho = Kc/L\Delta f. \qquad (18)$$

where c is speed of light, and K proportionality constant. The trade-off between effective bandwidth Δf and array length L for a small resolution angle ε is attractive in practice, especially, for the applications where signal attenuation due to the propagation media is severe for the higher frequencies [4].

Conclusions

Impulse-type waveforms used for UWB radar applications can analytically be represented by a gneralized Gaussain pulse having a realizable energy density spectrum. Active-array beamforming based on impulse waveforms yields directional distortion in the energy spectrum of the received and combined signals. The directional distortion of impulse waveforms is a useful feature for automatic beam steering. The directivity energy pattern of impulse-array systems is characterized by a narrow mainlobe and no sidelobes. The half-energy beamwidth of the directivity pattern defines the resolution angle as a decreasing function of the effective bandwidth and the array length. Such a relationship is attractive in practice, especially, for high-resolution imaging radar.

References

[1] Harmuth, Henning F., Raouf N. Boules, and Malek G.M. Hussain (1999), *Electromagnetic Signals:Reflection, Focusing, Distortion, and their Practical Applications.* New York: Kluwer Academic/Plenum.

[2] Taylor, James D. (Editor) (1995), *Introduction to Ultra–wideband Radar Systems.* Florida: CRC Press.

[3] Hussain, Malek G.M. (1998), "Ultra-wideband impulse radar—An overview of principles, *IEEE AES Magazine,* vol. 13, no. 9, pp. 9–14.

[4] Carin, Lawrence, Norbert Geng, Mark McClure, Jeffrey Sichina, and Lam Nguyen (1999), "Ultra-wideband synthetic-aperture radar for mine-field detection," *IEEE Antennas and Propagation Magazine,* vol. 41, no. 1, pp. 18–33.

[5] Win, Moe Z., and Robert A. Scholtz (1998), "Impulse Radio: How it works," *IEEE Communications Letter, vol. 2, no. 2, pp. 36–38.*

[6] Harmuth, Henning F. (1984), *Antennas and Waveguides for Nonsinusoidal Waves.* New York: Academic Press.

[7] Hussain, Malek G.M. (1988), "Antenna patterns of nonsinusoidal waves with the time variation of a Gaussian pulse—Part I", *IEEE Trans. Electromagn. Compat.*, vol. EMC-30, no. 4, pp. 504–512.

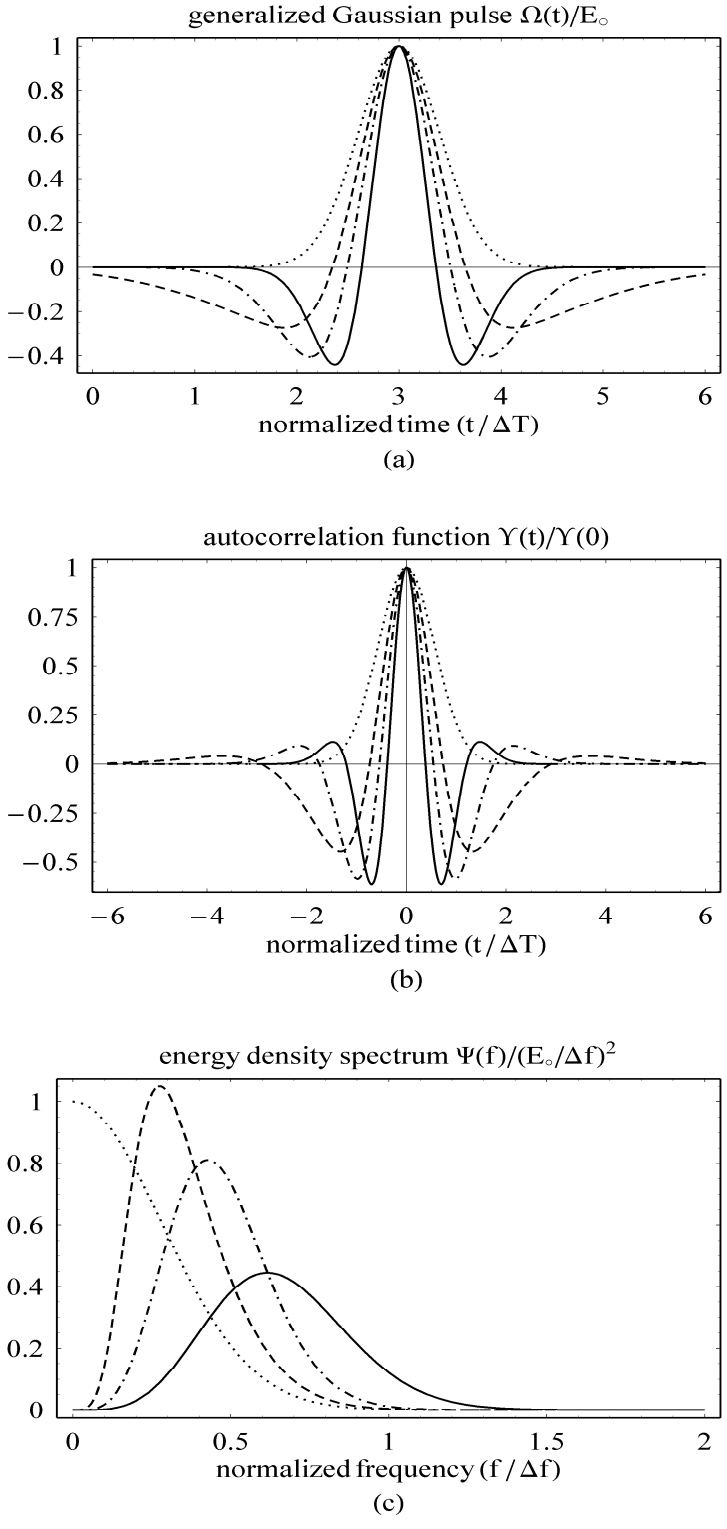

Figure 1. Normalized time variation of the generalized Gaussian pulse $\Omega(t)/E_\circ$ (a), autocorrelation function $\Upsilon(t)/\Upsilon(0)$ (b), and energy density spectrum $\Psi(f) = |\Lambda(f)|^2$ (c), for values of the scaling parameter $\alpha = 0$ (dotted line), $\alpha = 0.3$ (dashed line), $\alpha = 0.6$ (dashed-dotted line), and $\alpha = 1.2$ (solid line).

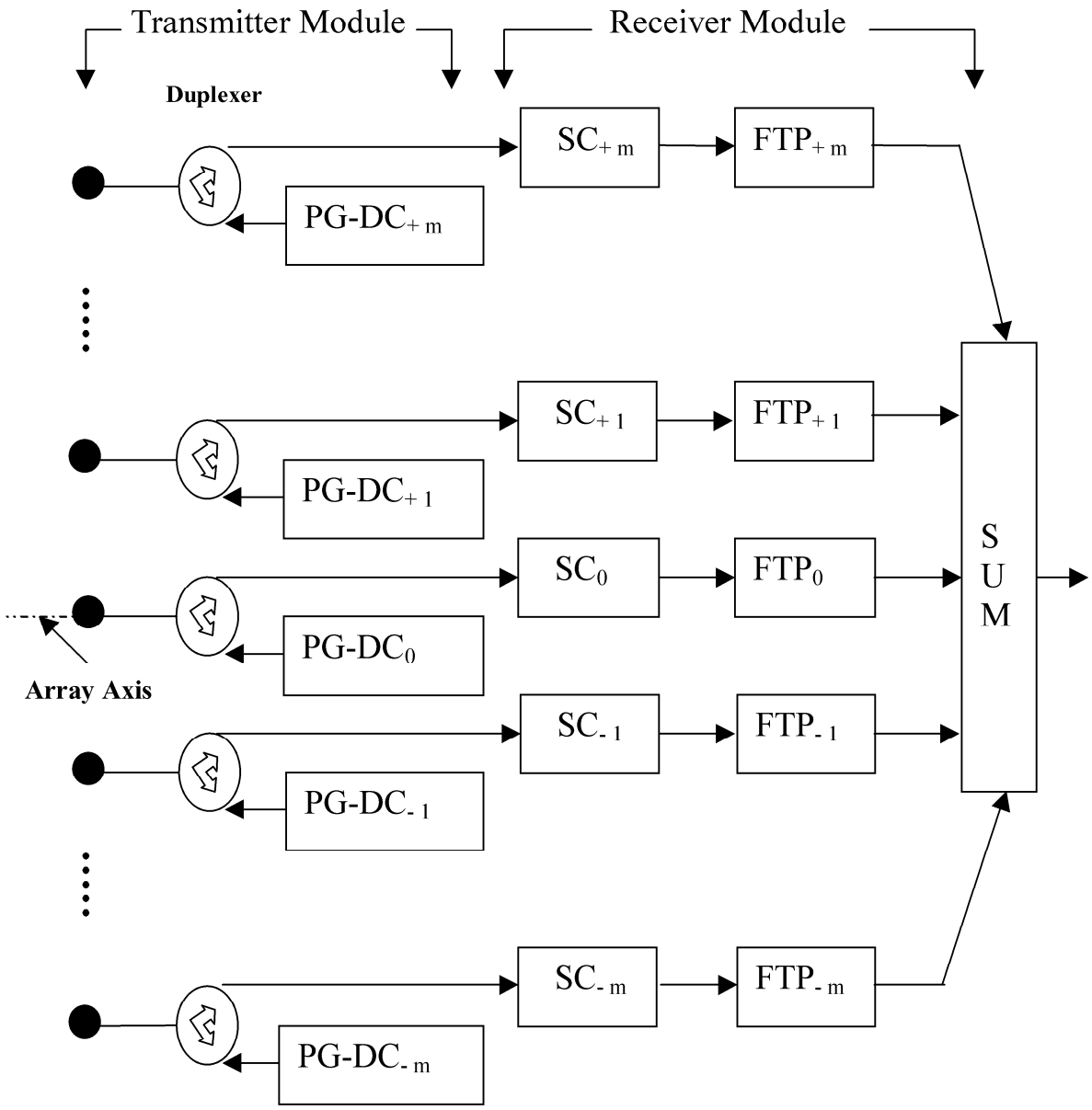

Figure 2. Active array beamforming system for UWB impulse radar. Each one of the $2m+1$ array elemnts is connected to a duplexer, pulse generator and driving circuits (PG-DC$_i$), sliding correlator (SC$_i$), Fourier transform processor (FTP$_i$), and summer circuit (SUM).

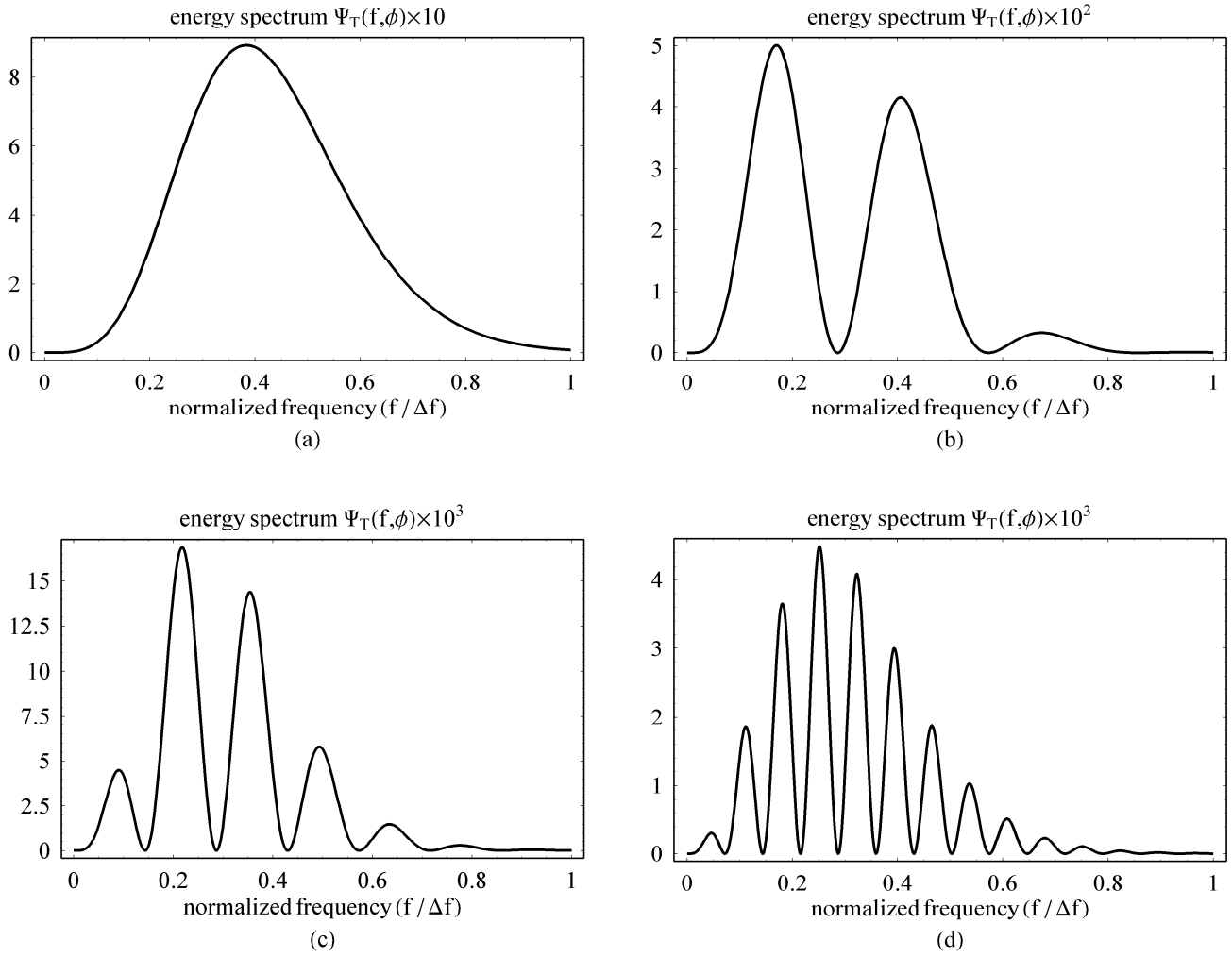

Figure 3. Energy density spectrum $\Psi_T(f,\phi)$ at the output of the beamforming system in Fig. 2 for $\alpha = 0.5$, $\rho = 100$, and the angle of incidence (a) $\phi = 0°$, (b) $\phi = 2°$, (c) $\phi = 4°$, and (d) $\phi = 8°$.

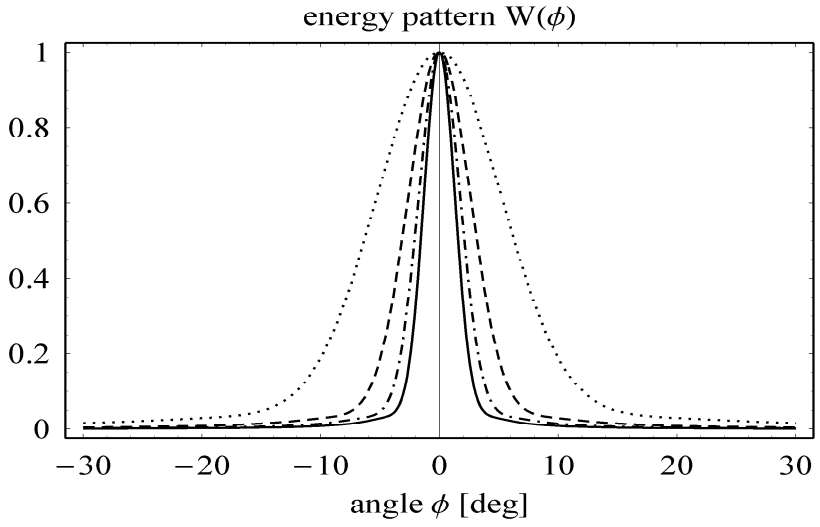

Figure 4. Directivity energy pattern $W(\phi)$ for the scaling parameter $\alpha = 0.5$, and the values of the spatial frequency bandwidth $\rho = 10$ (dotted line), 20 (dashed line), 30 (dashed-dotted line), and 40 (solid line).